Theoretical investigation of the structures of unsupported 38-atom CuPt clusters

Guerrero-Jordan, Josafat; Johnston, Roy L.; Cabellos, José Luis; Posada-Amarillas, Alvaro

DOI:
10.1140/epjb/e2018-90020-2

Theoretical Investigation of the Structures of Unsupported 38-atom CuPt Clusters

Josafat Guerrero-Jordan[1], José Luis Cabellos[2], Roy L. Johnston[3*]and Alvaro Posada-Amarillas[4*]

[1]Programa de Maestría en Ciencias (Física), División de Ciencias Exactas y Naturales, Universidad de Sonora, Blvd. Luis Encinas & Rosales, Col. Centro, 83000 Hermosillo, Sonora, México

[2]Departamento de Investigación en Polímeros y Materiales, Universidad de Sonora, Blvd. Luis Encinas & Rosales, Col. Centro, 83000 Hermosillo, Sonora, México

[3]School of Chemistry, University of Birmingham, Edgbaston, B15 2TT, Birmingham, UK

[4]Departamento de Investigación en Física, Universidad de Sonora, Blvd. Luis Encinas & Rosales, Col. Centro, 83000 Hermosillo, Sonora, México

*Authors for correspondence:

e-mail: posada@cifus.uson.mx

e-mail: r.l.johnston@bham.ac.uk

Abstract

A genetic algorithm has been used to perform a global sampling of the potential energy surface in the search for the lowest-energy structures of unsupported 38-atom Cu-Pt clusters. Structural details of bimetallic Cu-Pt nanoparticles are analyzed as a function of their chemical composition and the parameters of the Gupta potential, which is used to mimic the interatomic interactions. The symmetrical weighting of all parameters used in this work strongly influences the chemical ordering patterns and, consequently, cluster morphologies. The most stable structures are those corresponding to potentials weighted toward Pt characteristics, leading to Cu-Pt mixing for a weighting factor of 0.7. This reproduces DFT results for Cu-Pt clusters of this size. For several weighting factor values, the $Cu_{30}Pt_8$ cluster exhibits slightly higher relative stability. The copper-rich $Cu_{32}Pt_6$ cluster was reoptimized at the DFT level to validate the reliability of the empirical approach, which predicts a Pt@Cu core-shell segregated cluster. A general increase of interatomic distances is observed in the DFT calculations, which is greater in the Pt core. After cluster relaxation, structural changes are identified through the pair distribution function. For the majority of weighting factors and compositions, the truncated octahedron geometry is energetically preferred at the Gupta potential level of theory.

Keywords: Nanoalloys, Structural properties, Copper-Platinum clusters, Genetic algorithms

1. Introduction

Nanoalloys are materials with unique characteristics, which arise from their finite size, shape, and chemical composition. By controlling the size, composition and degree of chemical ordering (the degree of mixing or segregation of the component metals), the chemical and physical properties of these novel materials can be tuned [1-5], thus allowing tailoring of characteristics which are important for specific industrial applications. One of the main industrial applications of bimetallic nanoparticles, and therefore one of the major scientific challenges, is the catalytic conversion of exhaust gases such as CO and NO_x, generated as products of incomplete combustion in car engines and other industrial processes. The existence of multiple step catalytic reactions in pollution cleaning processes necessitates the development of new and more effective catalysts for multistep processes, where each metal may contribute to a different elementary step [6].

Transition and noble metal nanoalloy catalysts have shown exceptional activity for a number of important chemical reactions [7,8], which has been attributed to electronic and/or geometric effects [9,10]. This connection between composition and/or morphological details and chemical properties has been explored in several computational studies aimed at the rational design of nanocatalysts [11-13]. Experimental evidence for supported Pt-M (M = Au, Cu, Ni) nanoalloys reveals that the random alloy structures [8] exhibit superior catalytic activity for CO oxidation in comparison with conventional supported Pt catalysts. Several reports indicate that Cu-Pt nanoalloys are easily synthesized using methods which allow the tuning of particle size and shape [14-17]. On the theoretical side, there have been many studies of binary metallic clusters and a number of papers have been published aimed at

understanding the relationship between structural and chemical order and their physicochemical properties [3].

Many investigations have used semiempirical potentials to model the interatomic interaction [18-20], while others have adopted more advanced theoretical approaches such as Density Functional Theory (DFT) to study free or supported nanoparticles [21-25]. A disadvantage of first principles-based methods is that only small clusters can be studied because of their demanding computational resources. However, a combined approach can be used to study larger clusters as long as the global search, using a semiempirical potential, appropriately reproduces the structural motifs found experimentally. This combined methodology also requires well-developed computational strategies for energy landscape exploration based on empirical potentials, such as basin-hopping or genetic algorithm global optimization techniques, which can be applied to study large clusters – up to the nanoscale regime.

In this study, heteronuclear 38-atom Cu-Pt clusters are investigated, as a function of composition, using a genetic algorithm (GA) which incorporates the semiempirical Gupta potential [26], for which, experimental measurements on structural and energetic physical observables are used to fit homoatomic interaction parameters [27]. However, cross-interaction parameters are sometimes difficult to optimize due to the lack of experimental information, e.g., phase diagrams, and several combining rules have been developed, for example for Lennard-Jones systems [28]. Thus, a strategy for obtaining Gupta potential heteroatomic parameters, by taking arithmetic average values of the homoatomic interactions, has been widely explored by some of the authors of this work, with reasonable results [29-33]. For the Cu-Pt interactions, a heuristic symmetrical weighting of all Gupta potential parameters (for Cu and Pt) is used in this work, with the aim of understanding the

effect of parameter variations on their chemical ordering and morphology. This analysis is interesting because different experimental techniques can be used to synthesize unusual (metastable) chemical ordering in nanoparticles, as well as particles with different shapes and morphologies and, therefore, different physical and chemical properties. Excess energies and chemical ordering parameters are calculated, as well as a structure map showing the structural diversity found in this study. Finally, DFT local minimization is performed on a representative isomer ($Cu_{32}Pt_6$) of C_{5v} symmetry, to validate our empirical potential approach, investigating possible effects of the electronic structure on cluster geometry. This Pt_{core}-Cu_{shell} copper-rich cluster was singled out due to the enhanced catalytic activity observed in Cu-Pt dealloyed nanoparticles [34] with high copper loading.

2. Computational Methodology

2.1. The Gupta Potential

The Gupta potential was originally designed to deal with inconsistencies between experimental data and pair potential predictions in metallic surfaces [35], and is now used to model interatomic interactions in many noble and transition-metal systems [27]. It is a semiempirical many body potential derived within the tight-binding second-moment approximation. In this interaction model, the configurational energy of a cluster is written as the sum over all the atoms of attractive and repulsive energy components:

$$V_{clus} = \sum_i^N \{V^r(i) - V^m(i)\} \quad (1)$$

where the Born-Mayer pair repulsive term $V^r(i)$ is expressed as:

$$V^r(i) = \sum_{j\neq i}^{N} A(\alpha,\beta)e^{-p(\alpha,\beta)\left(\frac{r_{ij}}{r_0(\alpha,\beta)}-1\right)} \quad (2)$$

and the many-body attractive term $V^m(i)$ is expressed as:

$$V^m(i) = \sqrt{\sum_{j\neq i}^{N} \xi^2(\alpha,\beta)e^{-2q(\alpha,\beta)\left(\frac{r_{ij}}{r_0(\alpha,\beta)}-1\right)}} \quad (3)$$

α and β represent the atomic species of atoms i and j, respectively. A, ξ, p and q are the potential parameters that are usually fitted to experimental properties of bulk metals and alloys, such as the cohesive energy, lattice parameters, and independent elastic constants for the reference crystal structure at 0 K; r_0 denotes the nearest neighbor distance of the pure bulk elements, the value of r_0 for the mixed interaction ($\alpha\neq\beta$) is often taken as the average of the pure metal distances but it can also be taken as the experimental nearest-neighbor distance in some specific ordered bulk alloy; and r_{ij} is the distance between atoms i and j [35]. Values of the Gupta potential parameters describing Pt-Pt and Cu-Cu interactions are taken from the work of Cleri and Rosato [27]. These values are listed in Table 1.

2.2. Parametrization of the Gupta Potential

A previous study on Pt-Pd nanoalloys concluded that parameters obtained by averaging the parameters of pure elements, gave a good qualitative fit to previous experimental and theoretical studies of this type of bimetallic clusters [30]. In the current study, the effect of potential parameter changes on the structures and chemical ordering of 38-atom Cu-Pt clusters is explored. The heteronuclear Cu-Pt Gupta potential parameter set $\{P\}$ is derived as the weighted average of the corresponding pure metal Cu-Cu and Pt-Pt

parameters. The weighting parameters have been investigated in the range $0 \leq w \leq 1$ in steps $\Delta w = 0.1$, i.e., from the value for Pt-Pt (w=0) to the value for Cu-Cu (w=1) [36]. This is called symmetrical weighting of all parameters. Therefore, the Gupta potential parameters $\{P\}$ = $\{A, \xi, p, q$ and $r_0\}$ are obtained as:

$$P(\text{Cu-Pt}) = wP(\text{Cu-Cu}) + (1 - w)P(\text{Pt-Pt}) \qquad (4)$$

This equation allows us to analyze different scenarios, in a systematic way and over all the composition range, where physical effects may intervene to modify the interatomic bond description through semiempirical potentials [37]. Table 2 shows the values used in this work.

It is worthwhile noting that potential parameters have been successfully tested against DFT calculations for a number of pure and bimetallic clusters, showing a significant ability to reproduce structural properties of nanosized systems, in particular segregation or mixing effects, using different computational methodologies [38,39]. Nevertheless, because of the vast number of possible bi- or multimetallic nanoparticles that can be synthesized, DFT confirmation has not been achieved yet in many relevant cases which, therefore, must initially be studied using empirical potentials. Thus, potential parameter exploration, such as that presented here, is an unavoidable first stage in theoretical studies of nanoalloys that look for the comprehension from an atomistic viewpoint of experimental observations. In this sense, the results obtained under the scheme proposed here must be considered good first estimates that have to be subjected to experimental confirmation in order to establish their predictive potential.

2.3. The Birmingham Cluster Genetic Algorithm

The Birmingham Cluster Genetic Algorithm (BCGA) is a program that has been used widely to find the putative local minima as well as other low-lying energy structures of mono- and bi-metallic clusters [29,36,40]. A detailed description of the methodology can be found elsewhere [26,41]. BCGA is used here to minimize the cluster potential energy (V_{clus}), thus the lowest energy clusters have the highest fitness and the highest energy clusters have the lowest fitness. Dynamic scaling is achieved by using a normalized value of the energy, ρ, in the fitness calculations:

$$\rho_i = (V_i - V_{min})/(V_{max} - V_{min}) \qquad (5)$$

where V_{min} and V_{max} are the lowest and highest energy clusters in the current population, respectively. The choice of fitness function controls how rapidly fitness falls off with increasing cluster energy. Much effort has been expended in optimizing the BCGA operations and parameters needed to perform the global search, further details can be found in [36].

Because of the stochastic nature of the GA, the BCGA program is run several times for each cluster composition and for each set of operations/parameters. It is generally found that there is not a great dependence of the success rate of finding the global minimum structure on the type of fitness function used, though even small improvements are useful, especially for large clusters. For larger clusters, a larger population size and maximum number of generations are generally required [26]. In our searches we limited runs to a maximum of 400 generations and a population of 40 clusters. For a given cluster size, 38 atoms in our case, coordinates of the atoms are randomly generated and normalized. It is

worth mentioning that an ab initio BCGA code has been developed and successfully tested on a number of small gas-phase and supported clusters, including clusters of up to 20 atoms [42]. However, due to the computational requirements of global optimization algorithms, it is still necessary to use empirical potential methodologies combined with higher theoretical level computations to study larger metal clusters and nanoalloys. Thus, it is still necessary to explore systematically the model potential parameters space to find those that reproduce experimental results.

2.4. Energetic and Structural Similarity Analysis

When studying fixed-size bimetallic clusters, the excess (or mixing) energy as a function of composition, Δ_N, is a useful quantity. For binary nanoalloys with fixed size (N = 38 atoms) but different compositions, Δ_N is defined as:

$$\Delta_N = E_N(A_M B_{N-M}) - M\frac{E_N(A_N)}{N} - (N-M)\frac{E_N(B_N)}{N} \qquad (6)$$

where $E_N(A_M B_{N-M})$ is the total energy of a given cluster calculated at the Gupta level and $E_N(A_N)$ and $E_N(B_N)$ are the total energies of the global minima of the pure metal clusters (i.e. Cu_N and Pt_N) [36]. This excess energy is an unbiased quantity, defined as zero for the global minima of the pure clusters. Negative values of Δ_N indicate that mixing is favorable. The lowest energy equilibrium structures are fed into eq. (6).

The structural similarity between the structures predicted by the Gupta potential, and the corresponding structures obtained through local DFT optimizations is assessed by means

of the root mean square deviation (RMSD) of the atomic positions, as defined by the following equation:

$$RMSD(A^{DFT}, A^{G}) = \sqrt{\frac{1}{n}\sum_{i=1}^{n}(A_{ix}^{DFT} - A_{ix}^{G})^2 + \left(A_{iy}^{DFT} - A_{iy}^{G}\right)^2 + (A_{iz}^{DFT} - A_{iz}^{G})^2} \quad (7)$$

where A^G is the corresponding cluster structure predicted by the Gupta potential, from which the A^{DFT} structure is obtained.

2.5. DFT Calculations

Previous studies on Cu-Pt clusters at the DFT level analyzed two specific compositions with truncated octahedral geometry [24]. In the present work, we have focused on the elucidation of local structural changes on the ground-state structure of the incomplete Mackay icosahedron $Cu_{32}Pt_6$ cluster, with C_{5v} symmetry. To this end, a local DFT reoptimization was carried out using the generalized gradient approximation (GGA) Perdew-Wang exchange–correlation functional (PW91) [43]. The calculations are performed using the triple zeta (TZ) quality basis set def-TZVP [44], which involves an overall combination of effective core potentials (ECP) and valence basis including relativistic effects for the description of platinum atoms, as implemented in the NWChem 5.1 quantum chemistry package [45]. Relativistic effects were not taken into account for copper atoms. In this paper, as in previous studies [24], symmetry restrictions are imposed in the relaxation procedure.

3. Results and Discussion

In order to gain reliable statistical information, one hundred minimum energy structures were obtained for each weighting and composition. In general, this procedure increases the likelihood of finding a diverse set of structural motifs. Those with the lowest energy are shown in Figure 1, which summarizes the structural variety as a function of composition and parameter weighting. Each square in the grid represents the minimum energy structure obtained for a given value of composition and weighting. For a given weighting, structures vary with composition in most cases. For w=0.0, the predominant structure is the truncated octahedron (TO) (Figure 2a). As the proportion of copper atoms increases, it is possible to identify other, lower symmetry motifs. These include the incomplete Mackay poly-icosahedron (iMpIh) (Figure 2b), the incomplete anti-Mackay poly-icosahedron (iaMpIh) and a few decahedral (Dh) symmetries. The pure copper cluster has the TO structure. For w=0.6 and w=0.7 we found exclusively TO structures for all compositions. For w=1.0 and w=0.9 a broad variety of the above-mentioned structures was found. These weightings also showed a higher degree of segregation, as shown in Figure 2c.

We calculated the excess energy for all weightings as a function of composition (Figure 3). The increase of excess energy as the weighting increases from w=0.0 to w=1.0 is clear. For compositions with a weighting factor of 0.7 and below, the excess energy is negative, indicating that mixing is favorable. The lowest values for every composition are those with weighting factor w=0.0. The lowest value is -44.0 eV and belongs to the composition $Cu_{26}Pt_{12}$. For w=0.8 the excess energy remains very close to zero. Weightings of 0.9 and 1.0 have all positive, yet small excess energy values. The highest value is 3.05 eV for w=1.0, corresponding to the composition $Cu_{20}Pt_{18}$. A critical analysis of the results shows

that weighting values close to 1.0 produce unrealistic segregation patterns and excess energy profiles. Furthermore, values of $w \leq 0.7$ reproduce the energetic preference of Cu and Pt atoms to mix, as obtained in previous DFT calculations on 38-atom TO Cu-Pt clusters [24]. In the current work, the energies of TO and iMpIh structures were particularly close when using a weighting factor of 0.6. Structures with slightly high relative stabilities are observed for $Cu_{30}Pt_8$ cluster, for values of the weighting factor from 0.0 to 0.4. Above 0.4, the peaks observed in this figure are significantly reduced. Interestingly, for these higher stability clusters the location of Pt atoms, occupying the center of hexagons or segregating into the cluster, maximizes the number of heteroatomic bonds. On the other hand, for w values of 0.5 and above, the number of heterogeneous bonds decreases markedly. Structural details are shown on Table 3.

In Figure 4, the relative energy of the TO and iMpIh structure types is plotted, with positive values corresponding to the TO energy being lower in energy than iMpIh. The figure shows that, though the iMpIh energy is never lower than the TO energy, their energies are approximately equal at the composition $Cu_{11}Pt_{27}$. In this study, the TO structure was selected for further analysis. For a better understanding of the energetics of the iMpIh and TO structures, we performed DFT calculations for both geometries of $Cu_{11}Pt_{27}$, the composition with the smallest energy difference ($\Delta E_{Gupta} \sim 0.06$ eV) at the Gupta potential level. At the DFT level, however, the energy difference $\Delta E_{DFT} \sim -0.444$ eV, meaning that the iMpIh structure is energetically preferred for the $Cu_{11}Pt_{27}$ cluster at this higher level of theory. Thus, even though semiempirical potentials may predict the correct chemical ordering for bimetallic clusters, prediction of the relative energetics of structural isomers requires calculation at a higher level of theory.

The chemical ordering of the clusters also varies with the Gupta potential parameter weighting and the cluster composition, with the weighting having the greatest influence. In general for structures with weighting values of 0.0-0.3, homogeneous mixing occurs (Figure 5a). Additionally, when there are very few Pt atoms, multi-core-shell structures (i.e. structural motifs comprising two or more fused polyhedra, each with a Pt core and a Cu shell) are evident (Figure 5b). We also found some layered structures for these values of *w* (Figure 5c). For weighting values of 0.4-0.7, copper atoms tend to occupy surface sites, thus producing simple Pt@Cu core-shell ordering when copper atoms cover the entire surface. On the other hand, for weighting values 0.8-1.0, a high degree of segregation is found, corresponding to so-called Janus particles, where the two metals have an approximately planar interface. It is worth mentioning that the range of values for *w*=0.1-0.3, reproduce the mixing tendency of 14-atom Cu-Pt clusters obtained in recent DFT computations [46]. Interestingly, mixed structures with TO symmetry are favored for Cu-poor clusters for weighting factors below 0.7, in agreement with DFT calculations performed on similar systems [47], while Pt@Cu segregation is found for weighting values of 0.4-0.7. This behavior can be rationalized in terms of the higher surface and cohesive energies of Pt compared to Cu, so that strong segregation is expected, producing clusters with Cu atoms on the surface. On the other hand, experimental results on bulk Cu-Pt alloys indicate that structural parameter values are closer to that of Pt, which permit us to dismiss *w* values close to 1.0, circumventing the possibility of finding unrealistic structures and chemical ordering in our searches.

Due to the dependence of the chemical ordering on the weighting factor value, we decided to investigate the *w* values for which the structures predicted by the semiempirical

Gupta potential are more similar to those obtained after DFT reoptimization. With this aim, 3 different *w* values were singled out (0.3, 0.7, 0.9), selecting the lowest energy structures predicted by the Gupta potential as input configurations to perform DFT reoptimizations. Three different compositions were explored for each *w* value, corresponding to the clusters $Cu_{18}Pt_{20}$, $Cu_{19}Pt_{19}$, and $Cu_{20}Pt_{18}$. DFT calculations were performed using the lowest multiplicity for each case. The RMSD between the structure obtained with the GA and that obtained after the DFT local optimization was calculated to assess the structural similarity. Table 4 shows the calculated RMSD values, indicating in general that, for each cluster, the higher structural similarity (lowest RMSD value) corresponds to $w = 0.3$. This index also exhibits a dependency on the composition and, possibly, on the cluster size. The latter is beyond the scope of this research.

It has recently been shown that, in Cu-Pt nanocrystals, electrocatalytic CO_2 reduction depends on composition, which is enhanced for higher copper atom loading [48]. Thus, in order to explore the effect produced when considering the cluster electronic structure, DFT calculations were performed for a copper-rich system ($Cu_{32}Pt_6$) as a representative model. DFT local minimization using the GGA PW91 functional did not dramatically change the structural motif used here (the core-shell $Cu_{32}Pt_6$ cluster produced for $w = 0.5$). Very small changes in the interatomic distances are found as a result of including more realistic interactions. A careful analysis of the optimization process shows an expansion of the Pt_6Cu_1 pentagonal bipyramid core, accompanied by a moderate expansion of the Cu_{31} shell, as well as a small contraction of the Pt-Cu core-shell distances. A more detailed study was carried out in order to understand the structural differences by calculating the Pair Distribution Functions (PDFs) of the corresponding GA and DFT minima, as shown in Figure 6 (ref. 49

for visualization tool). The PDF, g(r), is the probability of finding a pair of particles separated by a distance r, in a given volume [50]. In our current DFT results, the structural local distortions are manifested by a splitting in the second peak of g(r), which is not present for the structure obtained by modeling interatomic bonding through the Gupta empirical potential. Local distortions may be due to Jahn-Teller effects, which are expected to occur in small clusters [51].

4. Conclusions

We have performed a detailed analysis on the structure and chemical ordering of 38-atom Cu-Pt clusters, by varying the semiempirical Gupta potential parameters for the heteronuclear Cu-Pt interactions. Our results show that chemical ordering is highly dependent on the weighting factor (w), with different structural patterns being favored depending on the w value. We find that there is a greater variety of structures for parameters which are biased to Cu characteristics ($w \rightarrow 1$) or for Cu-rich compositions. Also a higher degree of segregation was found for high Cu weighting. For weighting values of 0.7 or lower, Cu-Pt mixing is favored, as indicated by the negative values of the excess energy. The most stable structures are those weighted towards Pt characteristics ($w \rightarrow 0$), for which a higher degree of mixing was observed. There is a preference for the TO geometry when there is an abundance of Pt atoms or parameters are weighted towards Pt. The structure map clearly shows a vast majority of weighting factors and compositions yielding TO clusters, which becomes the most likely morphology Cu-Pt clusters of this size.

A special case corresponds to the cluster $Cu_{11}Pt_{27}$, for which two competing structures (TO and iMpIh) are observed for a weighting factor of 0.6. For this composition, at the Gupta level, the optimized isomers (which have distinct structures and symmetries) are close in energy, with the TO structure slightly favored. However, DFT calculations predict energetic reordering of these isomers. In general, *w* values close to 1.0 produce unrealistic segregation patterns and excess energy profiles. For the Pt@Cu core-shell copper-rich $Cu_{32}Pt_6$ cluster, the DFT minimization shows an expansion of the Cu-Pt bonds, and slight local distortions are clearly exhibited through the second peak splitting in the pair distribution function. However, structural similarity analysis shows that the best fit to the DFT results is obtained for a weighting factor (w) of 0.3. This study also shows a dependency on cluster composition. A cluster size dependency is also possible and deserves further study in the future.

The procedure outlined in this investigation can be implemented for tuning empirical potential parameters to reproduce experimental observations of nanoalloy structures. This approach can be applied to a large number of binary clusters and nanoalloys using the Gupta potential, or other empirical potentials that model non-metal interactions, for example the Lennard-Jones potential [52]. The structures predicted using empirical potentials might be utilized as input configurations in studies with a higher level of theory, e. g., in the range of nanoparticle sizes (≥ 2 nm) where it is too computationally expensive to perform global searches at the DFT level, but where DFT local optimization and, calculation of physicochemical properties can be performed on ground-state and low-lying isomer structures, for example to explain the differences in catalytic performance found for particular CuPt nanoalloys [53].

Acknowledgements

JGJ acknowledges CONACYT for funding through a MSc scholarship to visit the School of Chemistry, University of Birmingham. APA is grateful to CONACYT for financial support through project 180424. The authors are grateful to J. Watkins for preliminary work and to Dr. P. S. West for helpful discussions. Some of the DFT calculations were realized on the High Performance Computing Area (ACARUS) of the Universidad de Sonora.

Author contribution statement

J. G.-J. Performed computations and prepared figures and tables.

R. L. J. planned and supervised the computational experiments and supervised the final version of the manuscript.

J. L. C. Carried out DFT high-performance computations and prepared figures, also contributing to the discussion of results.

A. P.-A. Conceived this research and wrote the manuscript with support of R. L. J.

All authors discussed the results.

References

1. R.L. Johnston, in *Atomic and Molecular Clusters* (Taylor and Francis, London and New York, 2002)

2. F. Baletto, R. Ferrando, Rev. Mod. Phys. **77**, 371 (2005)

3. R. Ferrando, R.L. Johnston, J. Jellinek, Chem. Rev. **108**, 845 (2008)

4. P.K. Jain, I.H. El-Sayed, M.A. El-Sayed, Nano Today **2**, 18 (2007)

5. J. Jellinek, in *Theory of Atomic and Molecular Clusters (*Springer, Berlin, 1999)

6. S. Zhou, B. Varughese, B. Eichhorn, G. Jackson, K. McIlwrath, Angew. Chem. Int. Ed. **44**, 4539 (2005)

7. M. Watanabe, J.S. Motoo, J. Electroanal. Chem. **60**, 267 (1975)

8. T.A. Yamamoto, T. Nakagawa, S. Seino, H. Nitani, Appl. Catal. A **387**, 195 (2010)

9. J.H. Sinfelt, G.D. Meitzner, Acc. Chem. Res. **26**, 1 (1993)

10. B. Roldan-Cuenya, Thin Solid Films **518**, 3127 (2010)

11. I. Czekaj, J. Wambach, O. Kröcher, Int. J. Mol. Sci. **10**, 4310 (2009)

12. J.K. Nørskov, T. Bligaard, T.J. Rossmeisl, C.H. Christensen, Nat. Chem. **1**, 37 (2009)

13. J.K. Nørskov, F. Abild-Pedersen, F. Studt, T. Bligaard, Proc. Nat. Acad. Sci. USA **108**, 937 (2011)

14. Q. Liu, Z. Yan, N.L. Henderson, J.C. Bauer, D.W. Goodman, J.D. Batteas, R.E. Schaak, J. Am. Chem. Soc. **131**, 5720 (2009)

15. M. Neergat, R. Rahul, J. Electrochem. Soc. **159**, F234 (2012)

16. W.Weihua, T. Xuelin, C. Kai, C. Gengyu, Colloids Surf. A **273**, 35 (2006)

17. X. Zheng, S. Liu, X. Chen, J. Cheng, C. Si, Z. Pan, A. Marcelli, W. Chu, Z. Wu, J. Phys.: Conf. Series **430**, 012037 (2013)

18. D.J. Borbón-González, R. Pacheco-Contreras, A. Posada-Amarillas, J.C. Schön, R.L. Johnston, J.M. Montejano-Carrizales, J. Phys. Chem. C **113**, 15904 (2009)

19. K. Yun, Y. Cho, P. Cha, J. Lee, H. Nam, J.S. Oh, J. Choi, S. Lee, Acta Mater. **60**, 4908 (2012)

20. A. Bruma, R. Ismail, L.O. Paz-Borbón, H. Arslan, G. Barcaro, A. Fortunelli, Z.Y. Li, R.L. Johnston, Nanoscale **5**, 646 (2013)

21. S. Dennler, J. Morillo, G.M. Pastor, J. Phys.: Condens. Matter **16**, S2263 (2004)

22. E. Apra, A. Fortunelli, J. Phys. Chem. A **107**, 2934 (2003)

23. O. Lopez-Acevedo, J. Akola, R.L. Whetten, H. Grönbeck, H. Häkkinen, J. Phys. Chem. C **113**, 5035 (2009)

24. P.S. West, R.L. Johnston, G. Barcaro, A. Fortunelli, J. Phys. Chem. C **114**, 19678 (2010)

25. L.O. Paz-Borbón, G. Barcaro, A. Fortunelli, S.V. Levchenko, Phys. Rev. B **85**, 155409 (2012)

26. R.L. Johnston, Dalton Trans. **32**, 4193 (2003)

27. F. Cleri, V. Rosato, Phys. Rev. B **48**, 22 (1993)

28. J. Delhommelle, P. Millié, Mol. Phys. **99**, 619 (2001)

29. L. O. Paz-Borbón, A. Gupta, R. L. Johnston, J. Mater. Chem. **18**, 4154 (2008)

30. C. Massen, T.V. Mortimer-Jones, R.L. Johnston, J. Chem. Soc. Dalton Trans. **23**, 4375 (2002)

31. L. O. Paz-Borbón, R. L. Johnston, G. Barcaro, A. Fortunelli, J. Phys. Chem. C **111**, 2936 (2007)

32. F. Pittaway, L. O. Paz-Borbón, R. L. Johnston, H. Arslan, R. Ferrando, C. Mottet, G.Barcaro, A. Fortunelli, J. Phys. Chem. C **113**, 9141 (2009)

33. R. Pacheco-Contreras, J. O. Juárez-Sánchez, M. Dessens-Félix, F. Aguilera-Granja, A. Fortunelli, A. Posada-Amarillas, Comp. Mater. Sci. **141**, 30 (2018)

34. P. Mani, R. Srivastava, P. Strasser, J. Phys. Chem. C **112**, 2770 (2008)

35. R.P. Gupta, Phys. Rev. B **23**, 6265 (1981)

36. R. Ismail, R.L. Johnston, Phys. Chem. Chem. Phys. **12**, 8607 (2010)

37. M. Cerbelaud, R. Ferrando, G. Barcaro, A. Fortunelli, Phys. Chem. Chem. Phys. **13**, 10232 (2011)

38. L. Peng, E. Ringe, R. P. Van Duyne, L. D. Marks, Phys. Chem. Chem. Phys. **17**, 27940 (2015)

39. J. Tang, L. Deng, S. Xiao, H. Deng, X. Zhang, W. Hu, J. Phys. Chem. C **119**, 21515 (2015).

40. L.O. Paz-Borbón, T.V. Mortimer-Jones, R.L. Johnston, A. Posada-Amarillas, G. Barcaro, A. Fortunelli, Phys. Chem. Chem. Phys. **9**, 5202 (2007)

41. C. Roberts, R.L. Johnston, N.T. Wilson, Theor. Chem. Acc. **104**, 123 (2000)

42. A. Shayeghi, D. Götz, J.B.A. Davis, R. Schäfer, R.L. Johnston, Phys. Chem. Chem. Phys. **17**, 2104 (2014)

43. J.P. Perdew, Y. Wang, Phys. Rev. B **45**, 13244 (1992)

44. K. Eichkorn, F. Weigend, O. Treutler, R. Ahlrichs, Theor. Chem. Acc. **97**, 119 (1997)

45. M. Valiev, E.J. Bylaska, N. Govind, K. Kowalski, T.P. Straatsma, H.J.J. van Dam, D. Wang, J. Nieplocha, E. Apra, T.L. Windus, W.A. de Jong, Comp. Phys. Comm. **181**, 1477 (2010)

46. A.S. Chaves, G.G. Rondina, M.J. Piotrowsky, J.L.F. Da Silva, Comp. Mater. Sci. **98**, 278 (2015)

47. S. Núñez, R.L. Johnston, J. Phys. Chem. C **114**, 13255 (2010)

48. X. Zhao, B. Luo, R. Long, C. Wang, Y. Xiong, J. Mater. Chem. A **3**, 4134 (2015)

49. A. Stukowski, Model. Simul. Mater. Sci. Eng. **18**, 015012 (2010)

50. D.A. McQuarrie, Statistical Mechanics, Harper and Row, New York (1976)

51. W.A. de Heer, Rev. Mod. Phys. **65**, 611 (1993)

52. X. Wu, J. Clust. Sci. **25**, 1615 (2014)

53. S. Lee, S. Jeong, W.D. Kim, S. Lee, K. Lee, W.K. Bae, J.H. Moon, S. Lee, D.C. Lee, Nanoscale **8**,10043 (2016)

Tables

Table 1. Gupta potential homonuclear parameters.

Parameter	**Cu-Cu**	**Pt-Pt**
A	0.0855	0.2975
ξ	1.224	2.695
p	10.960	10.612
q	2.278	4.004
r_0	2.556	2.775

Table 2. Cu-Pt Gupta potential parameter set values obtained from the symmetrical weighting approach.

w	**0.0**	**0.1**	**0.2**	**0.3**	**0.4**	**0.5**	**0.6**	**0.7**	**0.8**	**0.9**	**1.0**

A	0.2975	0.2763	0.2551	0.2339	0.2127	0.1915	0.1703	0.1491	0.1279	0.1067	0.0855
ξ	2.695	2.548	2.401	2.254	2.107	1.960	1.812	1.665	1.518	1.371	1.224
p	10.612	10.647	10.682	10.716	10.751	10.786	10.821	10.856	10.890	10.925	10.960
q	4.004	3.831	3.659	3.486	3.314	3.141	2.968	2.796	2.623	2.451	2.278
r_0	2.775	2.753	2.731	2.709	2.687	2.666	2.644	2.622	2.600	2.578	2.556

Table 3. Number of heterogeneous distances (NoHD) less than 2.6 Å for $Cu_{29}Pt_7$, $Cu_{30}Pt_8$, and $Cu_{31}Pt_7$ clusters. Representative weighting factor (*w*) values were selected.

Cluster	**NoHD**	***w***	**Geometry**

$Cu_{29}Pt_9$	76		TO
$Cu_{30}Pt_8$	72	0.2	TO
$Cu_{31}Pt_7$	66		low symmetry pIh
$Cu_{29}Pt_9$	62		TO
$Cu_{30}Pt_8$	64	0.4	iMpIh
$Cu_{31}Pt_7$	60		iMpIh
$Cu_{29}Pt_9$	54		TO
$Cu_{30}Pt_8$	54	0.7	TO
$Cu_{31}Pt_7$	51		TO

Table 4. RMSD (in Å) calculated between selected GA and DFT structures for three *w* values. This index is a measure of the structural expansion produced when the electronic structure is taken into account.

	w		
Cluster	**0.3**	**0.7**	**0.9**
$Cu_{18}Pt_{20}$	0.10	0.13	0.15
$Cu_{19}Pt_{19}$	0.13	0.14	0.12
$Cu_{20}Pt_{18}$	0.11	0.13	0.21

Figure captions

Figure 1. Structure map for all weightings and compositions of Cu_xPt_{38-x} clusters.

Figure 2. Three characteristic structures. (a) The TO was the most abundant structure found by the BCGA. (b) The iMpIh was also a common structure especially when copper concentrations are high. (c) A highly segregated (Janus-type) composition (note that this motif is not included in our results because it was not the one with the lowest energy).

Figure 3. Excess energy for all weightings and compositions.

Figure 4. Comparative plot between the energies of iMpIh and TO structures. $\Delta E_{iMpIh\text{-}TO}$ is the energy difference between these two structural motifs.

Figure 5. Mixing patterns of: (a) Structure $Cu_{18}Pt_{20}$ (w=0.1) displaying homogeneous mixing. (b) Structure $Cu_{34}Pt_4$ (w=0.0) is a multi-core shell structure with 4 cores of Pt. (c) Structure of $Cu_{19}Pt_{19}$ (w=0.1) exhibiting a layering profile.

Figure 6. Pair distribution function (g(r)) of $Cu_{32}Pt_6$ cluster (w=0.5). Small distortions are apparent by the second peak splitting exhibited in the DFT result. The inset shows top and bottom views of this cluster.

Figures

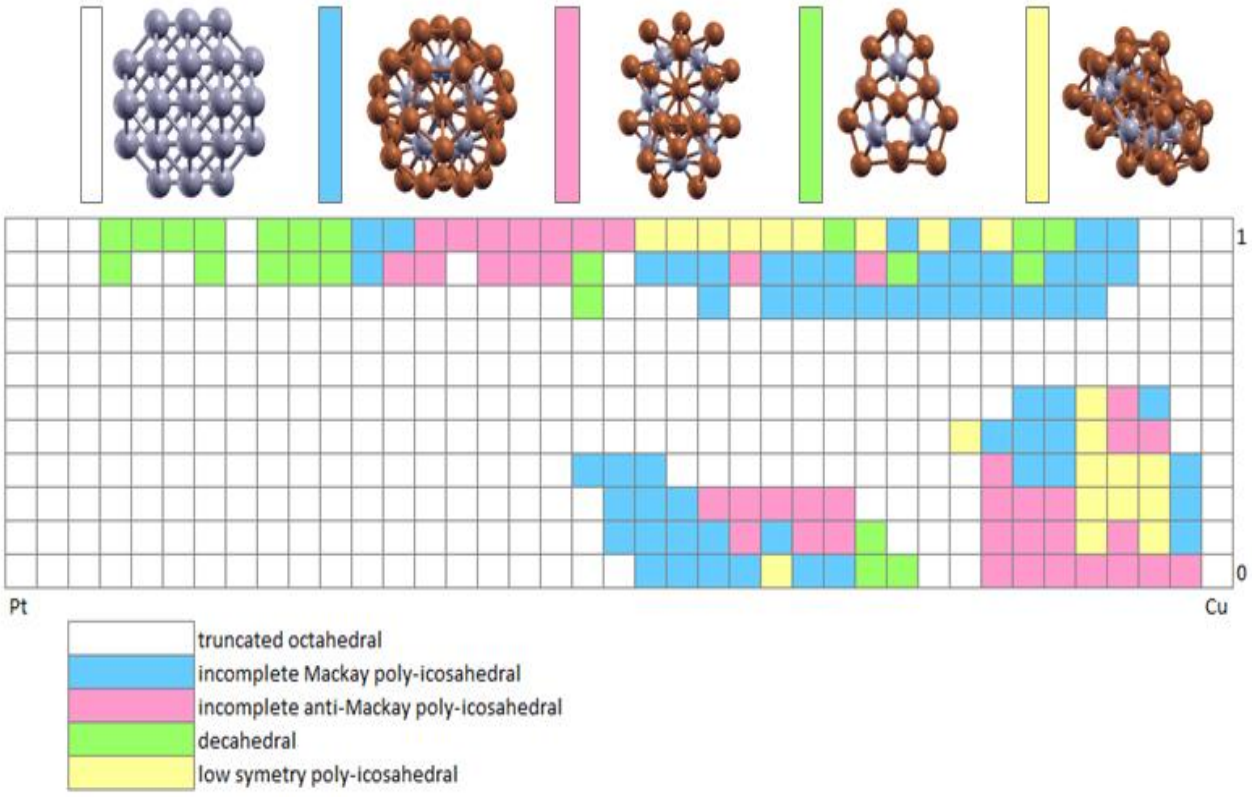
1
0
Pt
Cu
truncated octahedral
incomplete Mackay poly-icosahedral
incomplete anti-Mackay poly-icosahedral
decahedral
low symetry poly-icosahedral

Figure 1

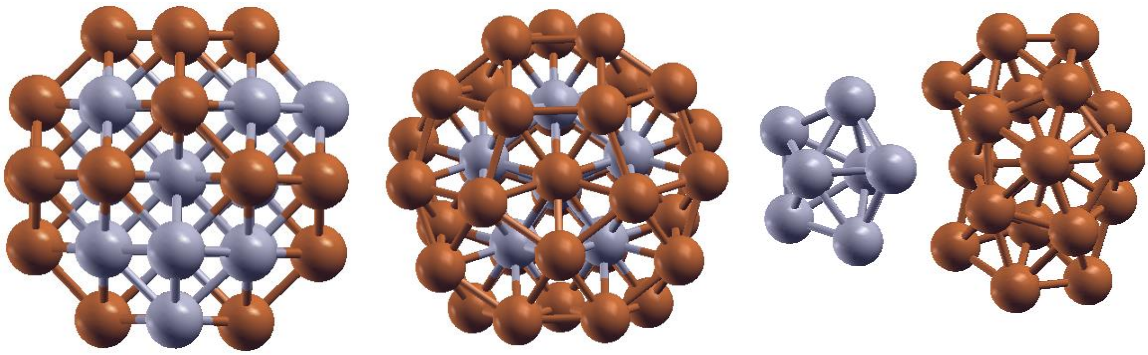

(a) **(b)** **(c)**

Figure 2

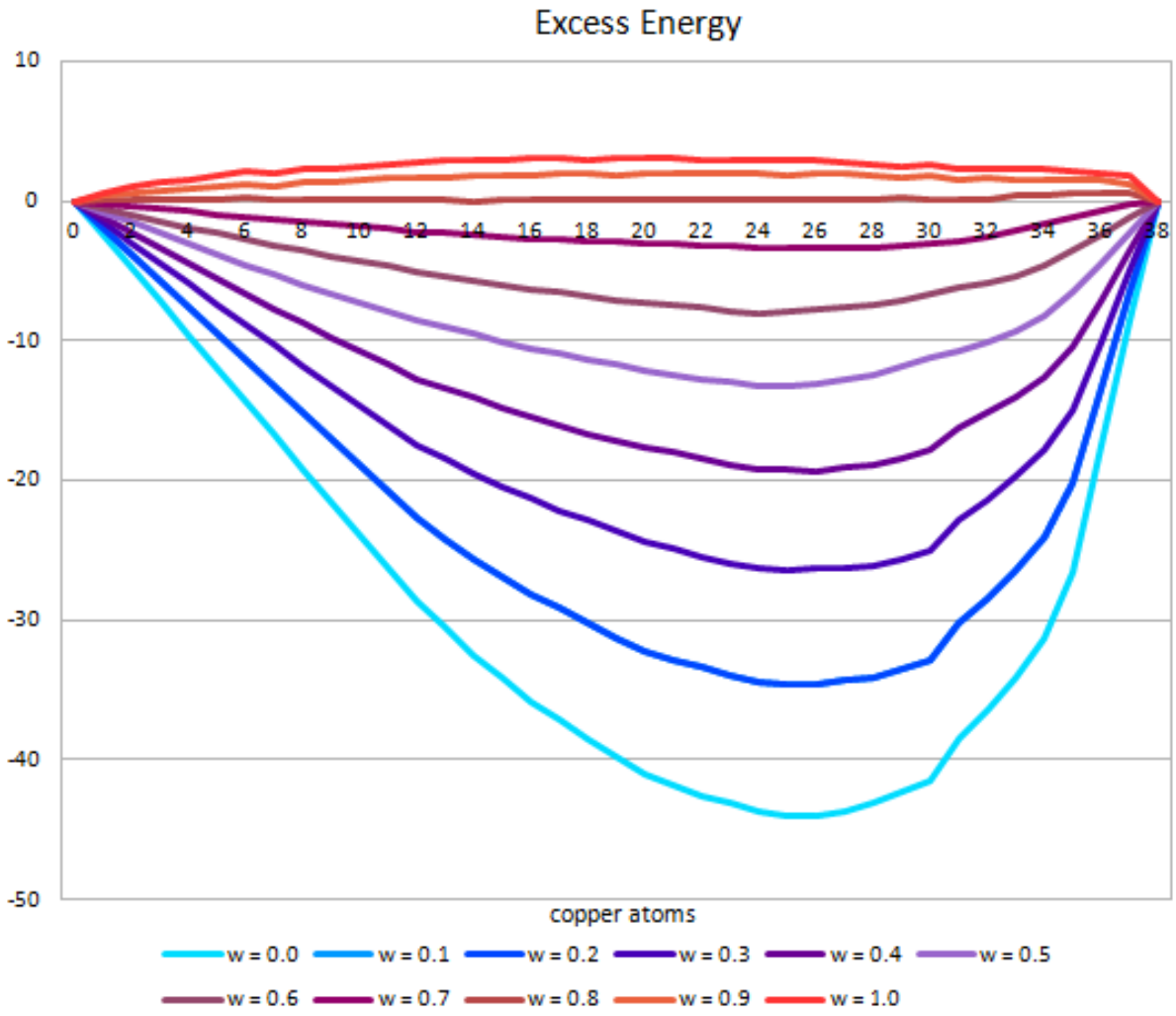
Excess Energy
10
0
-10
-20
-30
-40
-50
0
2
4
6
8
10
12
14
16
18
20
22
24
26
28
30
32
34
36
38
copper atoms
w = 0.0
w = 0.1
w = 0.2
w = 0.3
w = 0.4
w = 0.5
w = 0.6
w = 0.7
w = 0.8
w = 0.9
w = 1.0

Figure 3

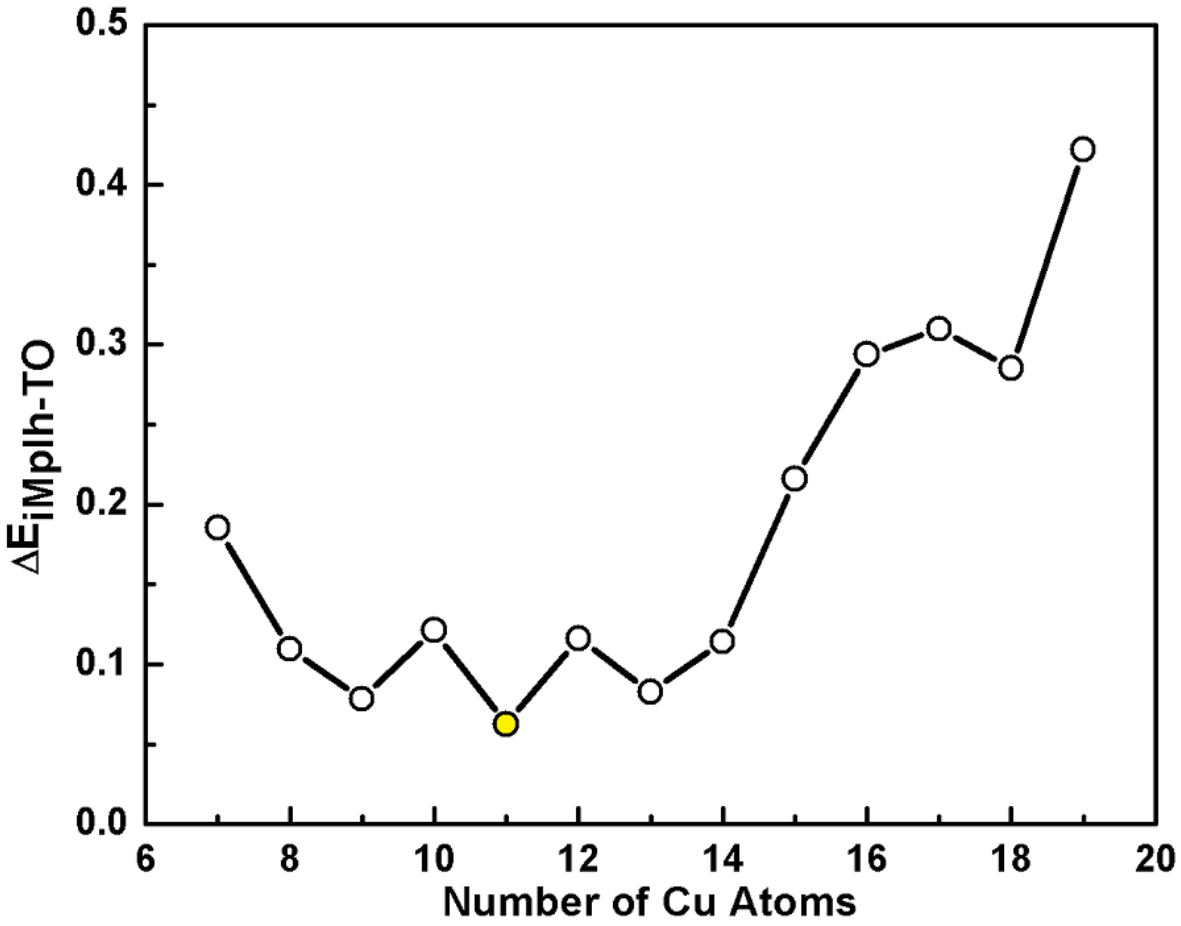
0.5
0.4
0.3
0.2
0.1
0.0
$\Delta E_{iMplh-TO}$
6
8
10
12
14
16
18
20
Number of Cu Atoms

Figure 4

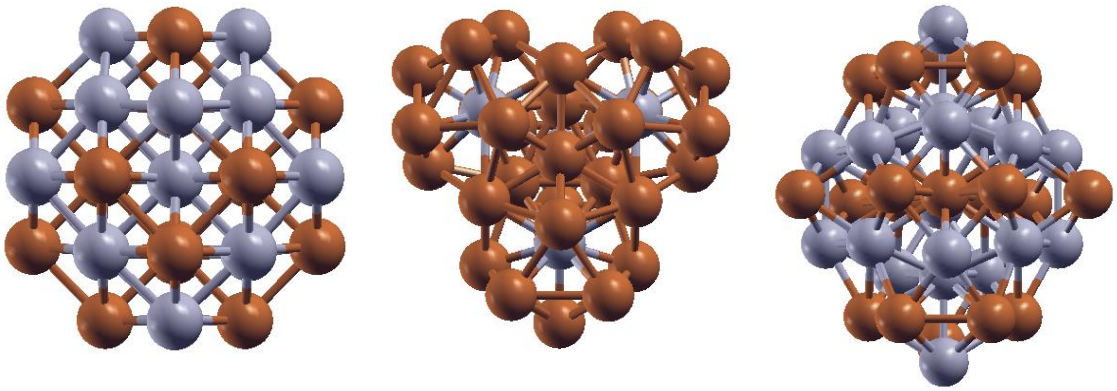

(a) **(b)** **(c)**

Figure 5

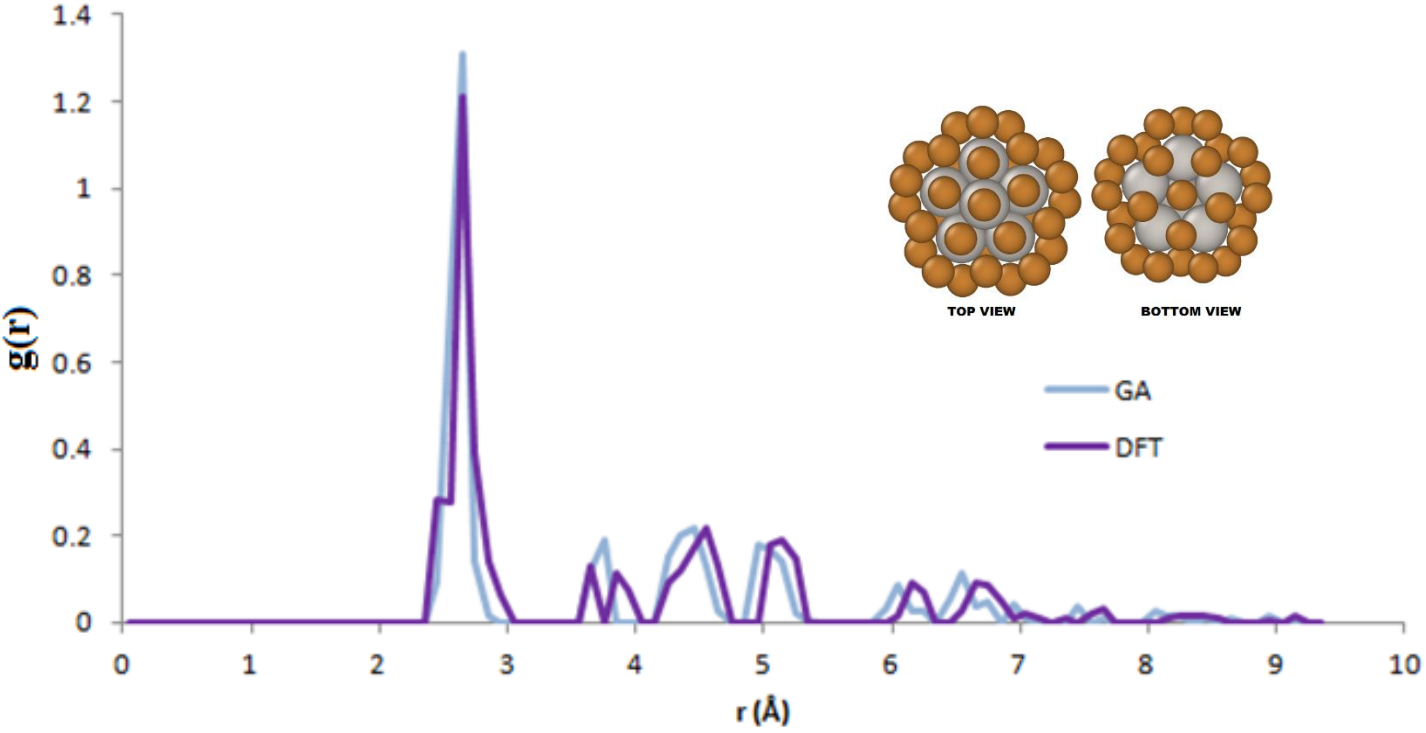
1.4
1.2
1
0.8
0.6
0.4
0.2
0
g(r)
0
1
2
3
4
5
6
7
8
9
10
r (Å)
TOP VIEW
BOTTOM VIEW
GA
DFT

Figure 6